Modeling acquired resistance to the second-generation androgen receptor antagonist enzalutamide in the TRAMP model of prostate cancer.

Marianna Cerasuolo[*1], Federica Maccarinelli*[2], Daniela Coltrini*[2], Ali Mokhtar Mahmoud[3], Viviana Marolda[3], Gaia Cristina Ghedini[2], Sara Rezzola[2], Arianna Giacomini[2], Luca Triggiani[4], Magdalena Kostrzewa[3], Roberta Verde[3], Debora Paris[3], Dominique Melck[3], Marco Presta[2], Alessia Ligresti[#3] and Roberto Ronca[#2]

[1] University of Portsmouth, School of Mathematics and Physics, Hampshire PO1 3HF, UK

[2] University of Brescia, Department of Molecular and Translational Medicine, Brescia, Italy.

[3] National Research Council of Italy, Institute of Biomolecular Chemistry, Pozzuoli, Italy.

[4] Department of Radiation Oncology, University and Spedali Civili Hospital, Brescia, Italy.

* These authors equally contributed to this work

Co-senior authorship

Running Title: Modeling enzalutamide resistance in prostate cancer

Keywords: TRAMP, prostate cancer, enzalutamide resistance, mathematical model

Correspondence to: Roberto Ronca, University of Brescia, viale Europa 11, 25123 Brescia, Italy. Tel +39-0303717735, FAX +39-0303717747. Email: roberto.ronca@unibs.it

Co-corresponding: Alessia Ligresti, National Research Council of Italy, Institute of Biomolecular Chemistry, Pozzuoli, Italy. Tel +390818675093, FAX +39 0818675340. Email: aligresti@icb.cnr.it

Conflict of interest disclosure: The authors declare no potential conflicts of interest.

ABSTRACT

Enzalutamide (MDV3100) is a potent second-generation androgen receptor antagonist approved for the treatment of castration-resistant prostate cancer (CRPC) in chemotherapy-naïve as well as in patients previously exposed to chemotherapy. However, resistance to enzalutamide and enzalutamide withdrawal syndrome have been reported. Thus, reliable and integrated preclinical models are required to elucidate the mechanisms of resistance and to assess therapeutic settings that may delay or prevent the onset of resistance.

In this study, the prostate cancer (PCa) multistage murine model TRAMP and TRAMP-derived cells have been used to extensively characterize in vitro and in vivo the response and resistance to enzalutamide. The therapeutic profile as well as the resistance onset were characterized and a multiscale stochastic mathematical model was proposed to link the in vitro and in vivo evolution of PCa. The model showed that all therapeutic strategies that use enzalutamide result in the onset of resistance. The model also showed that combination therapies can delay the onset of resistance to enzalutamide, and in the best scenario, can eliminate the disease. These results set the basis for the exploitation of this "TRAMP-based platform" to test novel therapeutic approaches and build further mathematical models of combination therapies to treat PCa and CRPC.

Significance:

Merging mathematical modeling with experimental data, this study presents the "TRAMP-based platform" as a novel experimental tool to study the in vitro and in vivo evolution of prostate cancer resistance to enzalutamide.

INTRODUCTION

Prostate cancer (PCa) represents a leading cause of death in the male population with around 180,890 new cases and 26,120 estimated deaths in the United States in 2016 [1].

Prostate development and PCa are androgen-dependent physiological and pathological contexts where Androgen Receptor (AR), acting as a ligand-dependent transcription factor [2], can initiate expression of genes controlling the balance between cell differentiation and proliferation. The prostatic epithelial AR signaling axis is a key regulator for the functionality, survival and differentiation of normal prostate [3]. In contrast, during carcinogenesis and prostate transformation, AR axis shifts toward a proliferative and tumor promoting gene set [4] due to aberrant activation by androgens, AR mutations/amplification, or changes in co-regulators interactions as well as signal pathways that activate AR activity at very low levels of androgen [5]. It is therefore crucial to inhibit androgen signaling either by depriving the tumor from androgens or by blocking the receptor activity.

To date, the androgen deprivation therapy (ADT) represents the standard care for the treatment of advanced PCa. Even though the suppression of androgens/AR functions is an effective treatment for most prostate cancer patients [6], clinical studies show that most prostate tumors regrow after a median duration of response of 12–24 months under continuous ADT and progress to what is termed as castration-resistance prostate cancer (CRPC) with an average survival of 2-3 years [7].

Although CRPC should be no longer controlled by androgen suppression, the clinical development of second-generation AR antagonists, which display higher affinity for the receptor as well as good efficacy as AR signaling inhibitor, has proven that the AR remains a critical oncogene in CRPC [8]. Indeed, preclinical evidence suggests that AR overexpression confers resistance to ADT *in vitro* [9], and that intra-tumoral levels of androgens are increased in patients with progressive PCa [10].

Enzalutamide (MDV3100, Xtandi®) is a non-steroidal second-generation AR inhibitor that competitively binds to the ligand-binding domain of the AR with higher affinity than conventional anti-androgens, impairs AR translocation to the nucleus, recruitment of cofactors, and binding to

DNA [11]. Enzalutamide has been associated with significant benefits in terms of prolonged survival in CRPC [12], although patients eventually experience disease progression. The mechanisms that underlie this resistance have not yet been clarified, and could be either dependent or independent from AR activity [13].

Many preclinical models of prostate cancer, mainly consisting of human or murine cell lines, are routinely used to assess the effect of different therapeutic approaches. However, none of these models fully recapitulates all the parameters of PCa progression in human disease, including formation of initial hyperplasia, intraepithelial neoplasia (PIN), adenocarcinoma, metastasis and recurrence from androgen deprivation therapy [14]. All these features of tumor onset and progression have been described in TRansgenic Adenocarcinoma of the Mouse Prostate (TRAMP) mice [15], a multistage prostate cancer model where the androgen-responsive rat probasin (*rPB*) gene promoter drives the prostate specific expression of the SV40-Tag. Prostate cancer in TRAMP mice mimics the development of human PCa, and transiently regresses following androgen withdrawal (e.g., by castration), but relapses as fatal androgen-independent PCa similar to what is commonly observed in men [16].

In this study, we characterized the response of TRAMP mouse as well as of TRAMP mouse-derived TRAMP-C2 cells to enzalutamide *in vitro* and *in vivo*, by generating *in vitro* enzalutamide-resistant TRAMP-C2 cells and by defining *in vivo* the therapeutic and relapse profile of enzalutamide in the multistage TRAMP model. The experimental evidence, together with the collected data, allowed the realization of a mathematical model that, for the first time, well describes the response and relapse to enzalutamide during tumor progression. The model suggested that resistant cells have a higher fitness than sensitive cells, and that the slow growth of resistant cells observed *in vitro* is compensated by their higher efficiency to grow under oxygen and glucose deprived conditions when *in vivo*. Finally, *in silico* experiments revealed that, regardless of time and/or treatment schedule, resistant cells take over, and combination treatments are required to delay tumor relapse.

MATERIALS AND METHODS

Cell lines. Murine prostate adenocarcinoma TRAMP-C2 cells were obtained from ATCC-LGC Standards Repository (ATCC number CRL-2731) and maintained in DMEM supplemented with 10% heat inactivated fetal calf serum (FCS), 10 mM HEPES Buffer, 0.5 mM 2-mercaptoethanol, 2.0 mM glutamine, 5 mg/L bovine insulin (Sigma-Aldrich) and 10 nM DHT. Cells were kept at low passage, returning to original frozen stocks every 3 to 4 months, and tested regularly for Mycoplasma negativity and morphology. Enzalutamide-resistant TRAMP-C2 cell line was generated culturing parental cells under increasing concentrations of enzalutamide (from 3μM up to 40μM) and maintaining the highest concentration up to 6 months. To verify the acquisition of resistant phenotype three parameters have been considered: 1) sensitivity to an acute treatment with enzalutamide via flow cytometry; 2) gene expression of castration resistant state biomarkers via PCR analysis; 3) metabolomics and extracellular flux analyses via NMR spectroscopy and Seahorse platform (see Supplementary Material and Methods). To exclude senescence related effects, a parental cell line, has been cultured in parallel with the same passage number to test the above parameters.

Cell proliferation assay. TRAMP-C2 cells were seeded in 48-well plates at 25,000 cells/cm^2 and treated with increasing concentrations (5-100μM) of enzalutamide (MDV3100 - Selleckchem). Cells were cultured under appropriate conditions for 96 hours. Propidium iodide staining (Immunostep, Salamanca, SP, EU) was used to detect PI- viable cells by flow cytometry. Absolute cell counts were obtained by the counting function of the MACSQuant Analyzer (Miltenyi Biotec).

Western Blot analysis. Cell samples were washed in cold PBS and homogenized in RIPA buffer containing 1% Triton-X100, 0.2% BriJ, 1 mM sodium orthovanadate and protease inhibitors cocktail. Protein concentrations were determined using the Bradford protein assay (Bio-Rad

Laboratories, Milano, Italy). Blotting analysis was performed using anti-AR, anti-phospho STAT3 and anti-STAT3 antibodies (Santa Cruz Biotechnology); anti-phospho Akt, anti-phospho ERK1/2 (Cell Signaling). To normalize the amount of loaded proteins, all blots were probed with anti–Tubulin antibody (Sigma).

Heterotopic tumor model. Animal experiments were approved by the local animal ethics committee (OPBA, Organismo Preposto al Benessere degli Animali, Università degli Studi di Brescia, Italy) and were performed in accordance with national guidelines and regulations. Nine week-old C57BL/6 male mice were injected s.c. with $5x10^6$ TRAMP-C2 cells in 200 µl total volume of PBS into the dorsolateral flank. When tumors were palpable (~80mm^3), mice were divided in two groups and treated or not with enzalutamide (3 mg/kg) in the drinking water. Treatments with everolimus (1 mg/kg) were performed every other day i.p., and with cabazitaxel (15 mg/kg) i.p. every two weeks. Tumors were measured in two dimensions and tumor volume was calculated according to the formula $V=(D \times d^2)/2$, where D and d are the major and minor perpendicular tumor diameters, respectively [17]. At the end of the experimental procedure tumors were removed, weighted and processed for histological analyses.

***In vivo* treatment of TRAMP mice.** TRAMP mice (C57BL/6-Tg(TRAMP)8247Ng/J) [18] were purchased from The Jackson Laboratory (Bar Harbor, ME, USA), bred crossing homozygous females with C57BL/6J wild type males and heterozygous TRAMP males were used for experimental procedures. Treatment was carried out adding enzalutamide (3 mg/kg) in the drinking water and treated or untreated mice were sacrificed at different time points, as indicated in the Results section, to collect the genitourinary apparatus that was weighted and prepared for histology. Treatment with cabazitaxel (15 mg/kg) was performed i.p. every two weeks.

Murine prostate histopathological analysis. The genitourinary apparatus was removed from wild-type or TRAMP male mice (treated or not with enzalutamide) at different ages, formalin-fixed and paraffin-embedded. Anterior prostate samples were sectioned at a thickness of 7μm, dewaxed, hydrated, and stained with hematoxylin and eosin (H&E) or processed for immunohistochemistry. Sections stained with H&E were evaluated for specific histological abnormalities. The full prostate section was acquired at 20x magnification with a Zeiss Axiovert 200M microscope (Carl Zeiss, Milan, Italy, EU) using the "Mosaic Tool" and the quantification of the pathological areas was performed with the AxioVision LE64 software. Also, the number of pathological adenomeres was determined and pathological areas were graded as described [19].

For the Immunohistochemical analysis, prostate sections were incubated with rat anti-mouse Ki67 antibodies (Dako, Milano, Italy, EU). Positive signal was revealed by 3,3'-diaminibenzidine (Roche) staining. Sections were finally counterstained with Mayer's hematoxylin before analysis by light microscopy. Images were acquired at 10x magnification with a Zeiss Axiovert 200M microscope and Image analysis was carried out using the ImagePro Plus software.

Statistical analyses. Statistical analyses were performed using the statistical package Prism 5 (GraphPad Software). Student's t test for unpaired data (2-tailed) was used to test the probability of significant differences between two groups of samples. Tumor volume data were statistically analyzed with a 2-way analysis of variance, and individual group comparisons were evaluated by the Bonferroni correction. Differences were considered significant when $P < 0.05$.

Formulation and parameterization of the Mathematical model.

The multiscale stochastic mathematical model presented in the quick guide describes PCa tumor cells dynamics *in vivo* and their response to treatment with enzalutamide. Drug resistance is a well-known issue in cancer patients' treatment, and in the last few years, many mathematical models have been proposed to fully understand the dynamics of the resistance and to find effective

therapeutic strategies to overcome it [20-22]. Recent experimental evidence suggests that tumor heterogeneity, tumor microenvironment and the ability of tumor cells to adapt to targeted therapy play a key role in the phenomenon of drug resistance [20, 23]. One of the consequences of heterogeneity is that within the same tumor there will be cells which are sensitive to drug therapy while others exhibit resistance to it [23], with this in mind we assumed that sensitive cells can undergo asymmetric cell division, resulting in resistant daughter cells. The development of the model was strongly led and supported by the experiments. To link the *in vitro* and *in vivo* results we incorporated the dynamics of the local tumor microenvironment, and how it affects the fitness of sensitive and resistant tumor cells. This was done by adapting previously developed spatial models of tumor growth [24, 25]. Values of cell-growth related parameters were obtained through the fitting of the experimental data. The nonlinear regression of data from the cell proliferation assay provided the values for the maximum growth rate coefficients of sensitive and resistant cells respectively, r_1=0.048 ± 0.009 hr^{-1} and r_2=0.038 ± 0.003 hr^{-1} (Supplementary Mathematical Model). The inhibition parameters b_1 = 0.064 ± 0.008 μM^{-1}, b_2 = 0.34 ± 0.3 and a_2 = 5.63 ± 5 μM were estimated with data from the experiments on the effect of different concentrations of enzalutamide on cell growth in starving conditions (Supplementary Mathematical Model). The empiric function proposed by Casciari et al. [24] to describe the impact of nutrients (oxygen and glucose) and pH on cell growth was used as it is. Although, the parameters representing the maximum environmental inhibition (C_{0i}, i=1,2) on cell growth were calibrated from fitting the *in vivo* cell growth data. Independent experiments showed that based on the concentration of enzalutamide in the environment, sensitive cells mutate into resistant cells and that the mutation is reversible. Such a phenomenon was modeled following the approach by Portz et al. [26] for the case of PCa cells treated with androgen deprivation therapies. Estimates of parameter values were obtained using independent experimental data (Supplementary Table S1). The equation for the pharmacokinetic of enzalutamide follows the one proposed by Sun et al. [22] for the dynamics of absorption, metabolism and elimination of a generic drug from the body. When the experiments were not

available the parameter values were collected from previous suitable studies [22, 24, 25]. More details on the parameterization can be found in the file Supplementary Mathematical Model.

RESULTS

Quick Guide to Equations and Assumptions.

Here we present a system of five stochastic differential equations that describe the interaction between heterogeneous cancer cell populations, the pharmacokinetics of the administered drug and the dynamics of the tumor microenvironment. The development of the system is based on *in vivo* experiments on TRAMP mice, and *in vitro* experiments on TRAMP-C2 cells growing in a Petri dish. Most of the ideas presented in this model have been adapted from previous works on human PCa development [22, 27], and prostate tumor in TRAMP mice by Ibrahim-Hashim [25] and Picco [28].

The model describes the growth of two populations of cancer cells: a drug sensitive population (S),

$$dS = \underbrace{\widetilde{r_S}\, S\,(1-g)\left(1-\frac{S+R}{K}\right)dt}_{Growth} - \underbrace{\widetilde{r_S}\, b_1 E\, S\, dt}_{Inhibition} - \underbrace{\widetilde{l_R}\, S\, dt}_{S\ to\ R} + \underbrace{\widetilde{l_S}\, R\, dt}_{R\ to\ S} - \underbrace{\mu\, S\, dt}_{mortality} + \underbrace{\sigma_1 S\, dW_1}_{Diffusion}$$

(E.1)

and a drug resistant population (R) [22, 28]

$$dR = \underbrace{\widetilde{r_S}\, g\, S\, dt}_{\substack{S\ asymmetrical \\ cell\ division}} + \underbrace{\widetilde{r_R}\, R\, \left(1-\frac{S+R}{K}\right) dt}_{Growth} - \underbrace{\widetilde{r_R}\frac{b_2 E}{a_2+E} R\, dt}_{Inhibition} + \underbrace{\widetilde{l_R}\, S\, dt}_{S\ to\ R} - \underbrace{\widetilde{l_S}\, R\, dt}_{R\ to\ S} - \underbrace{\mu\, R\, dt}_{mortality} +$$

$$\underbrace{\sigma_2 R\, dW_2}_{Diffusion} \qquad \text{(E.2)}$$

The growth of drug-sensitive and -resistant cells are represented by the first term of equation (E.1) and (E.2), respectively. The two tumor cell populations follow a logistic growth with K being the shared carrying capacity, and $\widetilde{r_S}$ and $\widetilde{r_R}$ the growth rate coefficients of each cell type. Cell proliferation is assumed to be dependent on oxygen and pH levels. At this purpose the empiric function proposed by Casciari et al. [24] was adapted and used to model the parameters $\widetilde{r_S}$ and $\widetilde{r_R}$:

$$f_i(O,H) = G_{0i}\, \frac{O}{G_a+O} \left(\frac{1}{H}\right)^n,\ i=S,R$$

$$\widetilde{r_i} = r_i\, f_i(O,H),\ \ i = S,R.$$

The function f_i assumes values in [0,1] and represents the fraction of maximum growth that cells can achieve given a specific set of conditions. G_j (j=o, h) and n are empirical parameters, while the variables O and H are respectively the oxygen and hydrogen ion concentration.

The growth of the sensitive type cells is also assumed to be asymmetric, i.e., S cells can randomly divide into drug-resistant cells, with rate g. As suggested by the *in vitro* experiments the administered drug induces death in both populations with different inhibition laws. Following treatment, the drug-sensitive cells undergo drug-induced death following a mass action law with maximal death rate b_1. On the other hand, drug-resistant cells undergo drug-induced death following drug administration too, but in this case the dependence of the death rate on the drug concentration (E) follows a Michaelis-Menten law, with b_2 representing the maximal death rate, and a_2 representing the drug concentration at which the inhibition effect is half of its maximum (b_2). The presence of enzalutamide triggers a selective pressure on sensitive cells that consequently develop resistance to the drug with a rate $\widetilde{l_R}$, e.g. through epigenetic mutations. The phenomenon is reversible and in an environment with a low or no enzalutamide concentration, resistant cells convert to sensitive cells with a rate $\widetilde{l_S}$. In this last case S cells will likely stay sensitive. The mutation rates take the form of Hill equations [26] with

$\tilde{l}_S = \frac{c_s\, a_s}{a_s+E}$ and $\tilde{l}_R = \frac{c_r\, E}{a_r+E}$.

The R to S mutation rate, $\widetilde{l_S}$, is assumed to be an increasing function of enzalutamide. The higher the drug concentration is in the environment the more cells developing resistance following selective pressure. On the other hand, the S to R mutation rate, $\widetilde{l_R}$, is assumed to be a decreasing function of the drug concentration, that is, the less enzalutamide is in the environment the more R cells will mutate into sensitive type cells. Both sensitive and resistant cells die with rate μ. The last diffusion terms in both equation (E.1) and (E.2) represent a standard Brownian motion, or standard Wiener process, which models the stochastic fluctuation of cell numbers. The Wiener process is

described by the normally distributed random variable W(t), with mean zero and variance Δt. The parameters σ_i (i = 1, 2) represent the diffusion rates.

The dynamics of enzalutamide concentration in the body is represented by the following equation

$$dE = -\underbrace{h\,E\,dt}_{Degradation} + \underbrace{V(t)\,dt}_{Delivery} + \underbrace{\sigma_3 E\,dW_3}_{Diffusion}. \quad \text{(E.3)}$$

The drug degrades with a maximum rate *h* and is delivered with a time dependent rate *V(t)* defined by the therapy. As for the populations, also in this case a Wiener process describes the stochasticity of the system [29].

This model represents the metabolic behaviour of the cells as dependent on the micro-environmental conditions, which are described by the two diffusible variables: oxygen (*O*) and extracellular pH modeled in terms of hydrogen ion concentration (*H*). The drift functions for *O* and *H* are those suggested by Ibrahim-Hashim et al. [25] and Robertson-Tessi et al. [30]. A constant oxygen input is assumed to feed the extracellular (considered equal to intracellular) oxygen concentration at any time.

$$dO = \underbrace{O_i\,dt}_{Oxygen\ input} - \underbrace{\frac{S}{(S+R)}V_{01}\,\frac{O}{O+k_0}\,dt}_{Oxygen\ consumption\ of\ S\ cells} - \underbrace{\frac{R}{(S+R)}V_{02}\,\frac{O}{O+k_0}\,dt}_{Oxygen\ consumption\ of\ R\ cells} + \underbrace{\sigma_4 O\,dW_4}_{Diffusion}.$$

(E.4)

Maximum oxygen consumption rates, V_{01} and V_{02} are characteristic of the cell type, sensitive and resistant cells respectively. According to Robertson-Tessi et al. proton dynamics depends on the amount of anaerobic glycolysis. A parameter p_G characterizes the cell type. Normal cells using an aerobic glycolysis would have $p_G = 1$, while for tumor cells $p_G > 1$ indicating that more glucose would be used to meet ATP demand. The normal target of ATP production rate is given by $\frac{29}{5}V_{01}$.

$$d\,H = \underbrace{\frac{S}{(S+R)}\,k_H\left(\frac{29}{5}\left(p_{G1}V_{01} - V_{01}\,\frac{O}{O+k_0}\right)\right)dt + \frac{R}{(S+R)}\,k_H\left(\frac{29}{5}\left(p_{G2}V_{02} - V_{02}\,\frac{O}{O+k_0}\right)\right)dt}_{Proton\ production\ by\ S\ and\ R\ cells} +$$

$$\underbrace{\sigma_5 H\,dW_5}_{Diffusion}. \quad \text{(E.5)}$$

As in equations (E.1), (E.2) and (E.3), also in equations (E.4), and (E.5) W_i are Wiener processes with σ_i (i = 4, 5) representing the diffusion rates.

Additional equations and parameterization details are reported in the Supplementary Mathematical Model.

Enzalutamide impairs murine prostate cancer cell growth in vitro and in vivo.

TRAMP-C2 cells represent a prototypic murine androgen-dependent prostate cancer cell line derived from the multistage TRAMP mouse model. As shown in Figure 1A, a 4-day treatment with increasing concentrations of enzalutamide strongly reduced cell proliferation, with an IC_{50} ~24μM, with no induction of cell death (Supplementary Figure S1). Western blot analysis revealed that the proliferative impairment is accompanied by reduction of STAT3, AKT and $ERK_{1/2}$ activation (Figure 1B). In agreement with other studies performed in human PCa cells [31], no significant reduction in AR protein levels was detectable after four days of treatment with enzalutamide (Figure 1B).

To further assess the therapeutic potential of enzalutamide *in vivo*, TRAMP-C2 cells were injected subcutaneously in syngeneic male mice. When tumors reached a size equal to ~80mm^3, mice were treated or not with 3 mg/kg of enzalutamide in the drinking water. As shown in Figure 1C-D, treatment with enzalutamide significantly delayed and reduced tumor volume, resulting in an impairment of tumor growth when compared to the control group.

Enzalutamide delays tumor onset and progression in TRAMP mice.

In the C57BL/6 background of the multistage TRAMP model, the age-dependent transformation of the prostate starts at 8-10 weeks with prostatic intraepithelial neoplasia (PIN) and progresses to well differentiated carcinoma and poorly differentiated adenocarcinoma [32]. The therapeutic potential of enzalutamide was tested in the TRAMP model by treating mice with 3 mg/kg of enzalutamide in

the drinking water starting from 12 weeks of age, when tumor onset has already started. Then, animals were examined for prostate tumor growth at 18, 22, 25 and 30 weeks.

As shown in Figure 2A, the weight of the genitourinary (GU) apparatus of TRAMP mice increases over time following tumor progression, reflecting tumor burden and organ oversizing/impairment. In enzalutamide-treated mice, the GU weight remains similar to that measured in healthy/wild type (WT) mice up to 22 weeks of age, starting to increase from week 25 and reaching the weight of the untreated TRAMP group at week 30.

Figure 2B shows representative H&E pictures of anterior prostate sections from wild-type (WT), TRAMP and enzalutamide-treated TRAMP mice at 18, 25 and 30 weeks. As described, the anterior prostate of WT mice has a normal morphology with alveolar gland lined by cubic epithelium with finger-like projections and the cells containing typically central nuclei. At variance, we observed a progressive increase of pathological areas in TRAMP mice, characterized by neoplastic proliferation of epithelial cells with nuclear atypia (hyperchromatic elongated nuclei or heterochromatic round nuclei). Indeed, smallest cells appear in several layers, they tend to occupy the gland lumen, even though at this stage the glandular architecture is still present.

In keeping with variations in the weight of the GU apparatus, histopathological analysis of the anterior prostate lobes revealed that the percentage of total pathological areas in untreated TRAMP mice increases from (17.4 ± 2.0)% at 12 weeks to (38.0 ± 3.9)% and (53.2 ± 3.7)% at 22 and 30 weeks of age, respectively (Figure 2C). This was paralleled by a decrease of normal/healthy (NH) prostatic tissue, an increase of PIN areas until week 22 and of well-differentiated (WD) carcinoma areas up to week 30 (Figure 2D). At variance, the percentage of total, PIN and WD pathological areas remains stable in the enzalutamide-treated TRAMP group at 18 and 22 weeks, to increase significantly thereafter (Figure 2C-D).

The early anti-tumor effect of enzalutamide observed at 18 weeks and the subsequent progressive transformation of TRAMP prostate occurring at week 25 was confirmed by the increase of proliferating/Ki67^{+} areas in enzalutamide-treated 25-week old mice (Figure 2E). Together, these

data indicate that the inhibitory effect exerted by enzalutamide on TRAMP tumor progression is progressively lost from week 25 onward.

Model prediction of tumor kinetics and onset of resistance following enzalutamide treatments.

The in vitro and in vivo data where used to develop the mathematical model described in the quick guide, and allowed investigating the dynamics of sensitive (S) and resistant (R) cells *in silico* with and without enzalutamide treatment.

As shown in Figure 3, the percentage of pathological area in the prostate of TRAMP mice (scattered dots) differently develops with time, in absence (A) and in presence (B) of enzalutamide continuous treatment. The mathematical model (blue continuous lines with 95% CI – orange and green continuous lines) recapitulates tumor growth, for instance ~94% of experimental observations fall in the 99.8% of the model simulations. The percentage of pathological area was calculated assuming that the maximum was reached at a volume of 1000 mm^3. The value was calculated from the estimated carrying capacity, K, by assuming a standard deviation of approximately 20% of K. Moreover, *in silico* prediction of the time course of tumor distributions show that the tumor increases constantly in time in the absence of treatment. From week 22, the tumor distribution reaches its maximum at around 500/600 mm^3 (Figure 3C). In the presence of enzalutamide treatment, the distribution is almost unchanged between week 12 and week 22, with a slight improvement at 18 weeks. However, the distribution shows that the tumor volume starts to increase at week 25 to continue in the following weeks (Figure 3D). Such behavior reflects the experimental evidence shown in Figure 2B.

The model suggests that untreated/control tumors are dominated by the growth dynamics of S cells, while enzalutamide-treated tumors are dominated by the switch from S to R cells and consequently by the dynamics of R cells.

Drug-induced mutation/transition, in the absence and in the presence of enzalutamide, is shown in terms of the dynamics of the proportion of S and R cells (dotted and continuous lines, respectively

in Figure 4A-B and in Supplementary Figure S2). On the contrary, in the presence of enzalutamide (Figure 4B), R cells arise and become the dominant population soon after the beginning of the treatment. This is explained by the fact that the inhospitable tumor microenvironment is characterized by increased acidity (with the pH varying from an initial value of 7.2 to a value in the range of 6.5 to 7.0), and a sensible decrease in oxygen (minimum 1.5%) while S cells invade the prostate (Supplementary Figure S3). In this more hostile context, drug-resistant cells have a fitness advantage when compared to their drug-sensitive parental cells, and this is not only due to the drug sensitivity and/or to the different mechanisms by which the drug acts on the cells, but also to the more effective way R cells respond to hypoxia and acidosis. Indeed, the reduction in growth of the R cells in the inhospitable environment is in fact less than half the reduction calculated for S cells.

In the attempt to find a "therapeutic window", our model was applied to evaluate *in silico* the cellular response to different treatment schedules with enzalutamide. The main aim was to decrease the number of S cells while avoiding the emergence of R cells. Three *in silico* experiments were performed, varying the dose and timing of enzalutamide administration, with no significant improvement in the therapeutic outcome (Figure 4C-E). In most of the conditions evaluated it was possible to control the growth of S cells, but not relevant effect was observed in the emergence of R cells that will dominate tumor growth (Figure 4C-E). A possible explanation is that even though high levels of enzalutamide are able to kill S cells, they cause a strong "metagenetic" response, with S cells mutating into the R type, which is capable of proliferating despite the adverse environmental conditions. *In silico* experiments also showed that, due to the heterogeneous nature of cancer cells, which implies that cells might develop some kind of resistance even in absence of enzalutamide, the use of lower levels of enzalutamide will not prevent the appearance of high fitness resistant cells and tumor relapse.

Enzalutamide-resistant TRAMP-C2 cells show CRPC markers and metabolic fitness

In order to mimic and better understand the emergence of enzalutamide resistance *in vivo*, we generated an enzalutamide-resistant cell line by culturing TRAMP-C2 cells in media gradually enriched with increasing concentrations of the drug (from 3μM to 40μM) up to 6 months. These resistant cells did not show morphological changes when compared to their aged-matched parental cells (Figure 5A). As evidence of the acquisition of enzalutamide-resistance features, qPCR analysis revealed a significant up-regulation of full-length AR mRNA and a strong down-modulation of TMEFF2 [33] and TMPRSS2 [34], two crucial modulators of the castration-resistant status in PCa [35] (Figure 5B). These data suggest that TRAMP-C2 cells efficiently overcome the ligand deficiency conferred by long-term enzalutamide treatment by elevating AR levels and decreasing androgen-dependent genes exerting anti-proliferative effects. Accordingly, enzalutamide-resistant TRAMP-C2 cells showed an increased IC_{50} (83μM) following an acute enzalutamide treatment when compared to aged-matched parental cells IC_{50} (24μM) (Figure 5C).

The *in vitro* characterization of enzalutamide-resistant TRAMP-C2 revealed that these cells were endowed with a reduced proliferative rate compared with their parental counterpart (Supplementary Mathematical Model). On the other hand, the mathematical model suggested that R cells appear to be much more efficient in dealing with oxygen deprived and lower pH conditions when grown *in vivo*, showing a higher fitness than S cells. For this reason, we further characterized enzalutamide-treated cells by measuring their main metabolic pathways with Seahorse analyzer. In particular, mitochondrial oxidative phosphorylation and glycolysis were measured simultaneously via OCR (oxygen consumption rate) and ECAR (extracellular acidification rate). The energy map based on extracellular flux analysis (Figure 5D) showed that enzalutamide-resistant cells have altered mitochondrial bioenergetics as indicated by reduction of oxidative phosphorylation and a distinct acidic phenotype, as indicated by their increased glycolysis capacity.

These findings are in keeping with the NMR-based metabolomics analysis that revealed conspicuous differences in metabolic profile between enzalutamide-resistant cells and their parental aged-matched cells (Figure 5E). Spectra acquisition show some hydrophilic signals commonly

identified as hallmark of castration resistant cell secretion, such as pyruvate and lactate, highly up regulated in resistant cells and indicating high glucose consumption (enhanced glycolysis) and hyper-acidosis. Metabolite analysis in resistant cells also indicated a lower ATP production and augmented levels of alanine, glycine, and other amino acids, indicating propensity in synthesizing amino acids. Moreover, the levels of several substrates used in TCA cycle by different mitochondria complexes, such as glutamate and succinate, were up regulated in resistant cells, thus indicating a reduced use of oxidative phosphorylation to produce energy in this phenotype.

Overall, these data were consistent with the topology-based pathway analysis, which indicated the metabolic networks potentially affected during the transition of TRAMP-C2 cells from an enzalutamide-sensitive to a resistant phenotype. As shown in Figure 5F, the most impacted metabolic pathways were related to alanine, aspartate and glutamate metabolism as specified by the volume and the color of the spheres (*yellow*, least relevant; *red*, most relevant) according to their statistical relevance P and impact value.

Model prediction and evaluation of enzalutamide-based combination therapies.

In order to overcome resistance to enzalutamide treatment we implemented the mathematical model to evaluate the effect of two clinically relevant drugs: everolimus, an mTOR inhibitor currently in clinical trial in combination with second-generation AR inhibitors [36], and cabazitaxel, a next-generation taxane approved for the treatment of metastatic CRPC in patients previously treated with docetaxel [37]. In vitro proliferation assays performed on parental and enzalutamide-resistant TRAMP-C2 cells were used to determine the IC_{50} and the dose response of both everolimus and cabazitaxel alone or in combination with enzalutamide (Figure 6A-D).

These data were used for the parametrization of the enriched mathematical model where both the equations of the new-drugs pharmacokinetic, and the interaction between enzalutamide and the two new drugs were considered (details in the Supplementary Mathematical Model). The model was run for the simulation of *in vivo* tumor growth under treatment with enzalutamide, everolimus and

cabazitaxel. The parameterization concerned the new functions and equations, while all other parameters stayed as previously evaluated. As shown in Figure 6E-F, treatment with enzalutamide *plus* cabazitaxel was expected to have a higher impact in delaying tumor growth, resulting in smaller tumors at the latest volume point considered for the simulation (>70 days).

We therefore validated the *in silico* drug combination to overcome the resistance to enzalutamide *in vivo*. An in vivo challenge on s.c. injected TRAMP-C2 cells confirmed that treatment with everolimus alone or in combination with enzalutamide resulted in no significant improvement in terms of anti-tumor activity when compared with enzalutamide given as single agent (Figure 7A). Interestingly, in agreement with the stochastic model simulation, treatment with cabazitaxel alone significantly delayed tumor growth when compared with enzalutamide, and the combination enzalutamide *plus* cabazitaxel emerged as the most effective therapeutic setting (Figure 7B).

As a proof of concept, the experimental tumor growth curves (represented by dots in Figure 6E-F) fall into the confidence intervals of the simulation in both combination treatments, revealing and confirming that enzalutamide *plus* cabazitaxel represents the best performing approach able to longer control tumor growth.

Prompted by the encouraging result obtained *in silico* and *in vivo*, we also run the simulation on the multistage tumor growth of TRAMP mice to predict the impact of the treatment on the evolution of the pathology. The model suggested that an *in vivo* enzalutamide *plus* cabazitaxel therapy would be successful in eliminating the tumor within 40 weeks (Figure 7C and Supplementary Figure S4). On this basis, TRAMP mice were treated with enzalutamide and cabazitaxel in single or combination regimens. As shown in Figure 7D, the enzalutamide *plus* cabazitaxel therapy exerted a significant impact on tumor growth, as assessed at the later time point considered (30 weeks), compared to single agent treatment. Accordingly, histopathological analysis (and GU/body weight ratio; Supplementary Figure S5) confirmed a significant impact of the combination regimen on tumor progression, resulting in very low (or no) pathological areas at the end of the experimental procedure (Figure 7D). Finally, a sensitivity analysis performed on several parameters revealed

that, depending on the considered drug combination, the system's behavior is more robust, in terms of the effect of the drug interaction, on either R or S cells. For each of the two introduced drugs the sensitive parameters would mostly refer to only one of the two phenotypes, and particularly to S cells for cabazitaxel and to R cells for everolimus (see Supplementary Figure S5 and Supplementary Mathematical Model).

DISCUSSION

As a leading cause of morbidity and mortality in men, prostate cancer has been widely studied and characterized in preclinical settings in order to bring therapeutic benefits to patients. Despite a first line response to canonical ADT and other new treatments, androgen independent tumors arise frequently with bad prognosis and poor therapeutic alternatives.

In this study, we characterized the full-time course of prostate tumors in response to enzalutamide taking advantage of the genetic murine TRAMP multistage model of PCa and related TRAMP-C2 cells *in vitro* and *in vivo*. Treatment with enzalutamide shows a significant effect on TRAMP-C2 cells both when cultured *in vitro* and when injected subcutaneously in syngeneic mice. Moreover, the therapeutic profile of enzalutamide-treated multistage TRAMP mice reveals that tumor progression is initially arrested for a significant time period (up to week 22 of age), when the percentage of pathological areas measured in the anterior prostate lobe is similar to that detectable in untreated TRAMP animals at week 12. Mirroring what happens in the clinics [13], long term administration of the drug resulted in the generation of enzalutamide-resistant TRAMP-C2 cells *in vitro*, and in the occurrence of tumor relapse both in subcutaneous TRAMP-C2 grafts and in multistage TRAMP mice *in vivo*. Indeed, TRAMP-C2 tumors start growing *in vivo* after a significant first line response. The amount of pathological areas in the prostate of TRAMP mice starts to increase at week 25, which represents the main "relapse time point" to be considered in enzalutamide-treatment experiments.

In a translational perspective, these TRAMP-integrated models represent a potential syngeneic platform to investigate the evolution of a therapeutic response to PCa and CRPC. Initial success and relapse are anticipated outcomes that resemble the clinical setting of PCa during its treatment. Different mechanisms have been found to be responsible for tumor progression after treatment with enzalutamide in murine and human models [38, 39]. AR alterations leading to androgen-independent activation, such as the AR-V7 variant [40] and the F876L mutant [41], have been identified and characterized in patients with progressive disease. Increase of glucocorticoid receptor

and transcription factors involved in the regulation of epithelial to mesenchymal transition (*i.e.* Twist and Snail) have also been described in human PCa cells treated with enzalutamide [42, 43]. Other bypassing mechanisms, including activation of PI3K/AKT pathway [44], increase of intra-tumor androgen biosynthesis through overexpression of AKR1C3 [45], or neuroendocrine/lineage switching following TP53 and RB1 alterations [46] have been associated with resistance to enzalutamide.

Notably, independently of the specific mechanism leading to resistance, in this work all data collected during *in vitro* and *in vivo* experiments were used for the first time to build a solid parametrization of growth conditions of PCa cells in the presence or absence of the therapeutic drug. Mathematical modeling of tumor behavior represents a seldom exploited, but extremely powerful and promising approach to investigate, and possibly predict, cancer ongoing and response in preclinical and clinical settings [47]. Studies conducted on PCa, colorectal and ovarian cancer (just to mention some of them) proved that by integrating empirical data with a mathematical framework of tumor growth it is possible to gain insights into the dynamics of intratumoral evolution [25, 26]; predict the effect of different combinations of drugs on patient survival rate [22, 48]; forecast the progression of the disease and develop personal adaptive therapeutic strategies [49]; and understand what strategies will be the most effective ones in controlling tumor growth [50].

Here, the mathematical analysis of tumor response describes how the number of drug-sensitive cells in pathological prostate adenomers decreases over time under enzalutamide-treatment conditions, while resistant cells outgrow and emerge as the predominant population. The numerical simulation nicely shows that this tendency is maintained over time in a high number (up to 1000) of realizations of the model, and regardless of the treatment schedule. Despite its first line efficacy, an enzalutamide-resistant cell subpopulation emerges and will emerge under different conditions. The mathematical model also shows how even if resistant cells exhibit a low rate of growth *in vitro*, they display a much higher fitness than their sensitive parental cells when grown *in vivo* under

suboptimal nutrient and pH conditions. This agrees with the major metabolic perturbations in amino acid metabolism and sugar-associated pathways observed in enzalutamide-resistant cells. In particular, resistant cells are endowed with increased levels of glutamate, succinate, alanine, glycine, taurine, pyruvate and lactate, while other metabolites, such as glutathione, UDP-N-acetylglucosamine and ATP, were down regulated in respect to their aged-matched parental cells.

Moreover, the implementation of the stochastic model allowed the evaluation of combination strategies aimed to overcome resistance or to improve the therapeutic profile/response. As a proof of concept, clinically relevant drugs (*i.e.* everolimus and cabazitaxel) resulted in different benefits in terms of anti-tumor activity, when combined with enzalutamide, and the mathematical simulation nicely predicted these experimental findings. For instance, in accordance with recently published clinical data, cabazitaxel alone showed a promising therapeutic profile [37], and the still unexplored combination enzalutamide *plus* cabazitaxel resulted as the best therapeutic setting to prolong survival and impact on tumor growth on both s.c. and multistage PCa models.

Interestingly, the interpretation of the sensitivity analysis results revealed that in combined treatments with enzalutamide (and *bona fide* with other drug candidates) the most sensitive parameters, which decide the outcome of the tumor growth, are the drug administered dose and the parameters representing the efficacy of the drug combination on either cell phenotype. Moreover, what emerged from this study is that no single parameter is reliably able to predict combination effects, and that to predict the therapeutic effect or the delay of tumor relapse it is necessary to focus on the combined effect of the interacting drugs (*i.e.* enzalutamide-cabazitaxel) on resistant cells. This aspect is of crucial importance and should be considered to screen and evaluate candidate drugs to be associated with enzalutamide or other first line therapies for the treatment of PCa and CRPC.

In conclusion, we implemented an integrated syngeneic “TRAMP-based platform” (see Graphical Abstract), widely exploited as a useful model to study PCa, by generating *in vitro* and *in vivo* enzalutamide-resistant cells, and by describing the evolution of PCa in response to second-

generation AR signaling blocker with a stochastic multiscale mathematical model. The outcome represents a powerful tool to test and validate new drugs to be used in combination with enzalutamide for the treatment of PCa and CRPC. The mathematical model described in this work can be used effectively to predict and validate the response of new drugs in PCa as well as to envision combination treatments following collection of new *in vitro* and *in vivo* evidence. Also, following existing approaches [22] the model can be easily integrated to account for the dynamics of multiple drugs and of metastatic cells. Once again, this study confirms that combination therapies remain the unmet strategy to be pursued in PCa treatment to avoid relapse and lethal progression of the disease. Future integrations of this mathematical model with clinical data from PCa patients and combination therapy parameters/equations could predict/evaluate the best treatment schedules to be used in CRPC treatment.

ACKNOWLEDGMENTS.

R.R. and M.P were supported by Associazione Italiana per la Ricerca sul Cancro (AIRC) MFAG 18459 and IG 1893 grants, respectively; A.G. was supported by Fondazione Cariplo (grant n° 2016-0570); S.R. was supported by an AIRC fellowship; A.M.M. and M.K. were supported by the INCIPIT PhD programme co-funded by the COFUND scheme Marie Skłodowska - Curie Actions.

REFERENCES

1. Siegel RL, Miller KD, Jemal A. Cancer statistics, 2016. CA Cancer J Clin. 2016;66:7-30.

2. Helsen C, Kerkhofs S, Clinckemalie L, Spans L, Laurent M, Boonen S, et al. Structural basis for nuclear hormone receptor DNA binding. Molecular and cellular endocrinology. 2012;348:411-7.

3. Isaacs JT, Furuya Y, Berges R. The role of androgen in the regulation of programmed cell death/apoptosis in normal and malignant prostatic tissue. Semin Cancer Biol. 1994;5:391-400.

4. Wang Q, Li W, Zhang Y, Yuan X, Xu K, Yu J, et al. Androgen receptor regulates a distinct transcription program in androgen-independent prostate cancer. Cell. 2009;138:245-56.

5. Niu Y, Altuwaijri S, Lai KP, Wu CT, Ricke WA, Messing EM, et al. Androgen receptor is a tumor suppressor and proliferator in prostate cancer. Proc Natl Acad Sci U S A. 2008;105:12182-7.

6. Miyamoto H, Messing EM, Chang C. Does androgen deprivation improve treatment outcomes in patients with low-risk and intermediate-risk prostate cancer? Nature clinical practice Oncology. 2005;2:236-7.

7. Beltran H, Beer TM, Carducci MA, de Bono J, Gleave M, Hussain M, et al. New therapies for castration-resistant prostate cancer: efficacy and safety. Eur Urol. 2011;60:279-90.

8. Beer TM, Armstrong AJ, Rathkopf DE, Loriot Y, Sternberg CN, Higano CS, et al. Enzalutamide in metastatic prostate cancer before chemotherapy. N Engl J Med. 2014;371:424-33.

9. Knudsen KE, Scher HI. Starving the addiction: new opportunities for durable suppression of AR signaling in prostate cancer. Clin Cancer Res. 2009;15:4792-8.

10. Montgomery RB, Mostaghel EA, Vessella R, Hess DL, Kalhorn TF, Higano CS, et al. Maintenance of intratumoral androgens in metastatic prostate cancer: a mechanism for castration-resistant tumor growth. Cancer Res. 2008;68:4447-54.

11. Tran C, Ouk S, Clegg NJ, Chen Y, Watson PA, Arora V, et al. Development of a second-generation antiandrogen for treatment of advanced prostate cancer. Science. 2009;324:787-90.

12. Cicero G, R DEL, Dorangricchia P, Dieli F. The Clinical Efficacy of Enzalutamide in Metastatic Prostate Cancer: Prospective Single-center Study. Anticancer Res. 2017;37:1475-80.

13. Claessens F, Helsen C, Prekovic S, Van den Broeck T, Spans L, Van Poppel H, et al. Emerging mechanisms of enzalutamide resistance in prostate cancer. Nature reviews Urology. 2014;11:712-6.

14. Gelman IH. How the TRAMP Model Revolutionized the Study of Prostate Cancer Progression. Cancer Res. 2016;76:6137-9.

15. Greenberg NM. Transgenic models for prostate cancer research. Urologic oncology. 1996;2:119-22.

16. Tang Y, Wang L, Goloubeva O, Khan MA, Zhang B, Hussain A. Divergent effects of castration on prostate cancer in TRAMP mice: possible implications for therapy. Clinical cancer research : an official journal of the American Association for Cancer Research. 2008;14:2936-43.

17. Giacomini A, Matarazzo S, Pagano K, Ragona L, Rezzola S, Corsini M, et al. A long pentraxin-3-derived pentapeptide for the therapy of FGF8b-driven steroid hormone-regulated cancers. Oncotarget. 2015;6:13790-802.

18. Greenberg NM, DeMayo F, Finegold MJ, Medina D, Tilley WD, Aspinall JO, et al. Prostate cancer in a transgenic mouse. Proc Natl Acad Sci U S A. 1995;92:3439-43.

19. Shappell SB, Thomas GV, Roberts RL, Herbert R, Ittmann MM, Rubin MA, et al. Prostate pathology of genetically engineered mice: definitions and classification. The consensus report from the Bar Harbor meeting of the Mouse Models of Human Cancer Consortium Prostate Pathology Committee. Cancer Res. 2004;64:2270-305.

20. Mumenthaler SM, Foo J, Choi NC, Heise N, Leder K, Agus DB, et al. The Impact of Microenvironmental Heterogeneity on the Evolution of Drug Resistance in Cancer Cells. Cancer Inform. 2015;14:19-31.

21. Lavi O, Gottesman MM, Levy D. The dynamics of drug resistance: A mathematical perspective. Drug Resist Update. 2012;15:90-7.

22. Sun XQ, Bao JG, Shao YZ. Mathematical Modeling of Therapy-induced Cancer Drug Resistance: Connecting Cancer Mechanisms to Population Survival Rates. Scientific reports. 2016;6.

23. Sun X, Hu B. Mathematical modeling and computational prediction of cancer drug resistance. Briefings in bioinformatics. 2017.

24. Casciari JJ, Sotirchos SV, Sutherland RM. Variations in Tumor-Cell Growth-Rates and Metabolism with Oxygen Concentration, Glucose-Concentration, and Extracellular Ph. Journal of cellular physiology. 1992;151:386-94.

25. Ibrahim-Hashim A, Robertson-Tessi M, Enriquez-Navas PM, Damaghi M, Balagurunathan Y, Wojtkowiak JW, et al. Defining Cancer Subpopulations by Adaptive Strategies Rather Than Molecular Properties Provides Novel Insights into Intratumoral Evolution. Cancer research. 2017;77:2242-54.

26. Portz T, Kuang Y, Nagy JD. A clinical data validated mathematical model of prostate cancer growth under intermittent androgen suppression therapy. Aip Adv. 2012;2.

27. Baez J, Kuang Y. Mathematical Models of Androgen Resistance in Prostate Cancer Patients under Intermittent Androgen Suppression Therapy. Appl Sci-Basel. 2016;6.

28. Picco N, Sahai E, Maini PK, Anderson ARA. Integrating Models to Quantify Environment-Mediated Drug Resistance. Cancer research. 2017;77:5409-18.

29. Leander J, Almquist J, Ahlstrom C, Gabrielsson J, Jirstrand M. Mixed Effects Modeling Using Stochastic Differential Equations: Illustrated by Pharmacokinetic Data of Nicotinic Acid in Obese Zucker Rats. Aaps J. 2015;17:586-96.

30. Robertson-Tessi M, Gillies RJ, Gatenby RA, Anderson AR. Impact of metabolic heterogeneity on tumor growth, invasion, and treatment outcomes. Cancer research. 2015;75:1567-79.

31. Rosati R, Chen B, Patki M, McFall T, Ou S, Heath E, et al. Hybrid Enzalutamide Derivatives with Histone Deacetylase Inhibitor Activity Decrease Heat Shock Protein 90 and

Androgen Receptor Levels and Inhibit Viability in Enzalutamide-Resistant C4-2 Prostate Cancer Cells. Mol Pharmacol. 2016;90:225-37.

32. Kaplan-Lefko PJ, Chen TM, Ittmann MM, Barrios RJ, Ayala GE, Huss WJ, et al. Pathobiology of autochthonous prostate cancer in a pre-clinical transgenic mouse model. Prostate. 2003;55:219-37.

33. Gery S, Sawyers CL, Agus DB, Said JW, Koeffler HP. TMEFF2 is an androgen-regulated gene exhibiting antiproliferative effects in prostate cancer cells. Oncogene. 2002;21:4739-46.

34. Yu J, Mani RS, Cao Q, Brenner CJ, Cao X, Wang X, et al. An integrated network of androgen receptor, polycomb, and TMPRSS2-ERG gene fusions in prostate cancer progression. Cancer cell. 2010;17:443-54.

35. Kregel S, Chen JL, Tom W, Krishnan V, Kach J, Brechka H, et al. Acquired resistance to the second-generation androgen receptor antagonist enzalutamide in castration-resistant prostate cancer. Oncotarget. 2016;7:26259-74.

36. Tucci M, Zichi C, Buttigliero C, Vignani F, Scagliotti GV, Di Maio M. Enzalutamide-resistant castration-resistant prostate cancer: challenges and solutions. OncoTargets and therapy. 2018;11:7353-68.

37. de Wit R, de Bono J, Sternberg CN, Fizazi K, Tombal B, Wulfing C, et al. Cabazitaxel versus Abiraterone or Enzalutamide in Metastatic Prostate Cancer. The New England journal of medicine. 2019.

38. Culig Z. Molecular Mechanisms of Enzalutamide Resistance in Prostate Cancer. Current molecular biology reports. 2017;3:230-5.

39. Vander Ark A, Cao J, Li X. Mechanisms and Approaches for Overcoming Enzalutamide Resistance in Prostate Cancer. Frontiers in oncology. 2018;8:180.

40. Scher HI, Graf RP, Schreiber NA, McLaughlin B, Lu D, Louw J, et al. Nuclear-specific AR-V7 Protein Localization is Necessary to Guide Treatment Selection in Metastatic Castration-resistant Prostate Cancer. European urology. 2017;71:874-82.

41. Korpal M, Korn JM, Gao X, Rakiec DP, Ruddy DA, Doshi S, et al. An F876L mutation in androgen receptor confers genetic and phenotypic resistance to MDV3100 (enzalutamide). Cancer discovery. 2013;3:1030-43.

42. Arora VK, Schenkein E, Murali R, Subudhi SK, Wongvipat J, Balbas MD, et al. Glucocorticoid receptor confers resistance to antiandrogens by bypassing androgen receptor blockade. Cell. 2013;155:1309-22.

43. Shiota M, Yokomizo A, Takeuchi A, Imada K, Kashiwagi E, Song Y, et al. Inhibition of protein kinase C/Twist1 signaling augments anticancer effects of androgen deprivation and enzalutamide in prostate cancer. Clinical cancer research : an official journal of the American Association for Cancer Research. 2014;20:951-61.

44. Carver BS, Chapinski C, Wongvipat J, Hieronymus H, Chen Y, Chandarlapaty S, et al. Reciprocal feedback regulation of PI3K and androgen receptor signaling in PTEN-deficient prostate cancer. Cancer cell. 2011;19:575-86.

45. Liu C, Lou W, Zhu Y, Yang JC, Nadiminty N, Gaikwad NW, et al. Intracrine Androgens and AKR1C3 Activation Confer Resistance to Enzalutamide in Prostate Cancer. Cancer research. 2015;75:1413-22.

46. Mu P, Zhang Z, Benelli M, Karthaus WR, Hoover E, Chen CC, et al. SOX2 promotes lineage plasticity and antiandrogen resistance in TP53- and RB1-deficient prostate cancer. Science. 2017;355:84-8.

47. Cerasuolo M, Paris D, Iannotti FA, Melck D, Verde R, Mazzarella E, et al. Neuroendocrine Transdifferentiation in Human Prostate Cancer Cells: An Integrated Approach. Cancer research. 2015;75:2975-86.

48. Zhang J, Cunningham JJ, Brown JS, Gatenby RA. Integrating evolutionary dynamics into treatment of metastatic castrate-resistant prostate cancer. Nature communications. 2017;8:1816.

49. Khan KH, Cunningham D, Werner B, Vlachogiannis G, Spiteri I, Heide T, et al. Longitudinal Liquid Biopsy and Mathematical Modeling of Clonal Evolution Forecast Time to

Treatment Failure in the PROSPECT-C Phase II Colorectal Cancer Clinical Trial. Cancer discovery. 2018;8:1270-85.

50. Kozlowska E, Farkkila A, Vallius T, Carpen O, Kemppainen J, Grenman S, et al. Mathematical Modeling Predicts Response to Chemotherapy and Drug Combinations in Ovarian Cancer. Cancer research. 2018;78:4036-44.

FIGURE LEGENDS

Figure 1. TRAMP-C2 cell response to enzalutamide *in vitro* and *in vivo*.

Cell proliferation (**A**) and Western blot analysis (**B**) on TRAMP-C2 cells treated with increasing concentrations of enzalutamide (Enza). DMSO was used as control, NT= not treated. **C**) In vivo tumor growth (pictures and tumor weight at the explant, in **D**) of subcutaneous TRAMP-C2 tumors. The arrow indicates treatment start (continuous oral administration); data are the mean ± SEM of 8-10 tumors/group; ** P<0.01, *** P<0.001).

Figure 2. Effect of enzalutamide in TRAMP mice.

A) Wild type (WT), TRAMP and enzalutamide-treated TRAMP mice were sacrificed at different time points (12, 18, 22, 25 and 30 weeks) and the genitourinary to body weight ratio determined. **B**) Representative picture (H&E) of anterior prostate lobes of Wild type, TRAMP and enzalutamide-treated TRAMP mice at 18, 25 and 30 weeks (scale bar: 100μm). **C**) Quantification (percentage) of the pathological area in the anterior prostate of TRAMP mice treated (+Enza) or not with enzalutamide. **D**) Histopathological evaluation of prostate tissue after explantation; the graph shows the percentage of normal healthy tissue (NH, in grey), prostatic intraepithelial neoplasia (PIN, in green) and well differentiated tumor area (WD, in white) in the prostate of untreated (-) or treated (+E) TRAMP mice. **E**) Representative pictures and quantification of $Ki67^{+}$ areas in prostate adenomers at 18 and 25 weeks (scale bar: 50μm). Data are the mean ± SEM; n= 8 or more animals/group; *p<0.05, **p<0.01, ***p<0.001.

Figure 3. Numerical simulations and time course of tumor distribution.

Plots **A** and **B** show how the percentage of pathological area in the prostate develops with time, in absence (**A**) and in presence (**B**) of enzalutamide continuous treatment. Starting from above the continuous lines represent the upper bound of the 3σ confidence interval (CI), the mean, and the

lower bound of the CI of all model realizations given the parameter values in Table S1. All points represent experimental data. Plots **Ca** and **Da** show 1000 realizations of the dynamics of enzalutamide-sensitive and -resistant tumor cells in time, described by the stochastic equations (E.1) and (E.2), in absence and presence of enzalutamide treatment respectively. Plots **C(b-f)** and **D(b-f)** represent the tumor distributions for the 1000 realizations in absence (A plots) and presence (B plots) of treatment at 12, 18, 22, 25 and 30 weeks.

Figure 4. Model of resistant cells onset and *in silico* simulation of enzalutamide treatment schedules.

Plots A and B show the behavior of the proportion of sensitive (dotted lines) and resistant cells (continuous lines) in absence (**A**) and presence (**B**) of enzalutamide over time. **C-E)** *In silico* experiments showing the effects on R (i=3) and S (i=2) cells number of three enzalutamide treatments (i=1). In Ci (i=1,2,3) increasing doses of enzalutamide (per week) are administered daily for 1 week followed by 2 weeks off. In Di (i=1,2,3) enzalutamide is administered daily for 2 weeks followed by 4 weeks off, with a higher dose during the first week. In Ei (i=1,2,3) enzalutamide is administered daily for 3 weeks followed by 3 weeks off with equal doses for each week.

Figure 5. Validation of enzalutamide resistance acquisition in TRAMPC2 cells.

A) Bright field microscopy images showing cell morphology of parental and enzalutamide-resistant TRAMP-C2 cells (magnification: 400X and 200X). **B**) qPCR analysis of the genes driving androgen deprivation resistance in enzalutamide-resistant cells (AR-FL: Androgen Receptor full-length, TMEFF2: Tomoregulin-2, TMPRSS2: transmembrane serine protease; *p <0.05, **p<0.01; t-test). **C**) Cell proliferation response of parental and enzalutamide-resistant TRAMP-C2 cells to increasing concentrations of enzalutamide. Data are shown as mean ± SEM of 3 independent experiments. **D**) Oxygen consumption rates (OCR) and extracellular acidification rates (ECAR) were determined using the Seahorse XF96 Analyzer in TRAMPC2 and enzalutamide-resistant cells.

Data are represented as the mean ± SEM (n=24). **E**) S-line plot generated by multivariate data analysis of the NMR spectra. Metabolic changes in enzalutamide-resistant cells compared with parental cells are shown in blue as the least significant changes and in red as the most significant. **F**) Topology-based pathway analysis showing metabolic networks mainly affected in enzalutamide-resistant cells according to their statistical relevance P and impact value.

Figure 6. Simulations of drug combinations to overcome resistance to enzalutamide.

In vitro cell proliferation assay performed on TRAMP-C2 parental or TRAMP-C2 enzalutamide-resistant cells to test everolimus (**A**), everolimus in combination with enzalutamide (**B**), or cabazitaxel alone (**C**) and in combination with enzalutamide (**D**). In silico simulation of enzalutamide *plus* everolimus (**E**) and enzalutamide *plus* cabazitaxel (**F**).

Figure 7. Validation of the *in silico* drug combinations to overcome the resistance to enzalutamide in vivo.

In vivo tumor growth of subcutaneous TRAMP-C2 tumors treated with enzalutamide *plus* everolimus (**A**) and enzalutamide *plus* cabazitaxel (**B**). Data are the mean ± SEM of 8-10 tumors/group). **C**) In silico simulation of tumor progression in TRAMP mice. **D**) In vivo: quantification (percentage) of the pathological area in the anterior prostate of TRAMP mice (at 30 weeks of age) treated with the indicated drugs and combination. * $P<0.05$, ** $P<0.01$, **** $P<0.0001$).

FIGURE 1

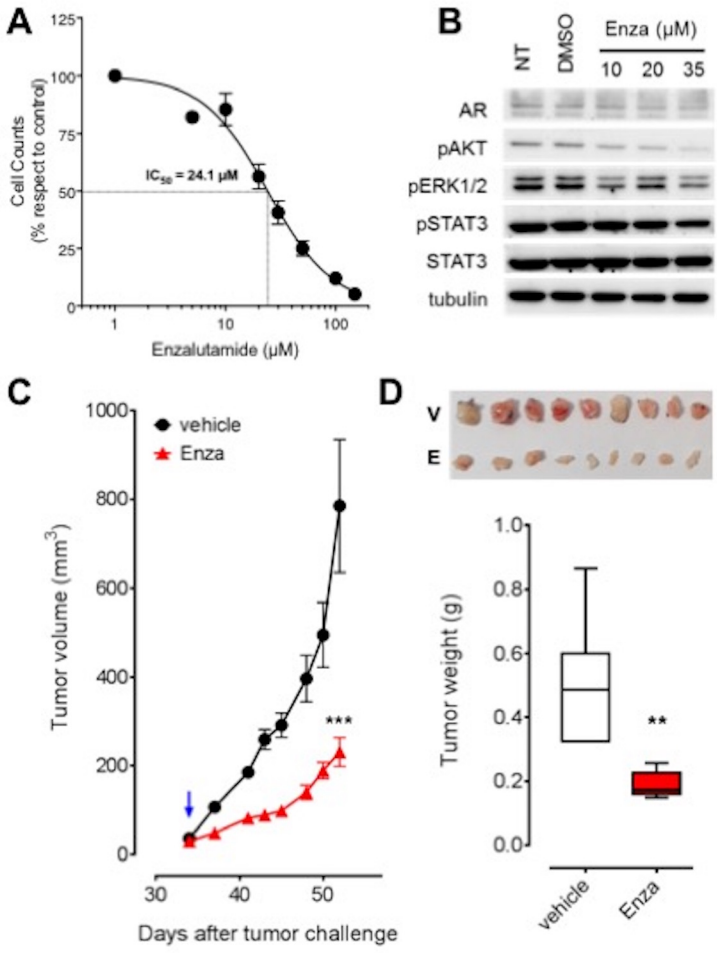
A
Cell Counts (% respect to control)
IC50 = 24.1 μM
Enzalutamide (μM)
B
NT
DMSO
Enza (μM)
10 20 35
AR
pAKT
pERK1/2
pSTAT3
STAT3
tubulin
C
vehicle
Enza
Tumor volume (mm3)
***
Days after tumor challenge
D
V
E
Tumor weight (g)
**
vehicle
Enza

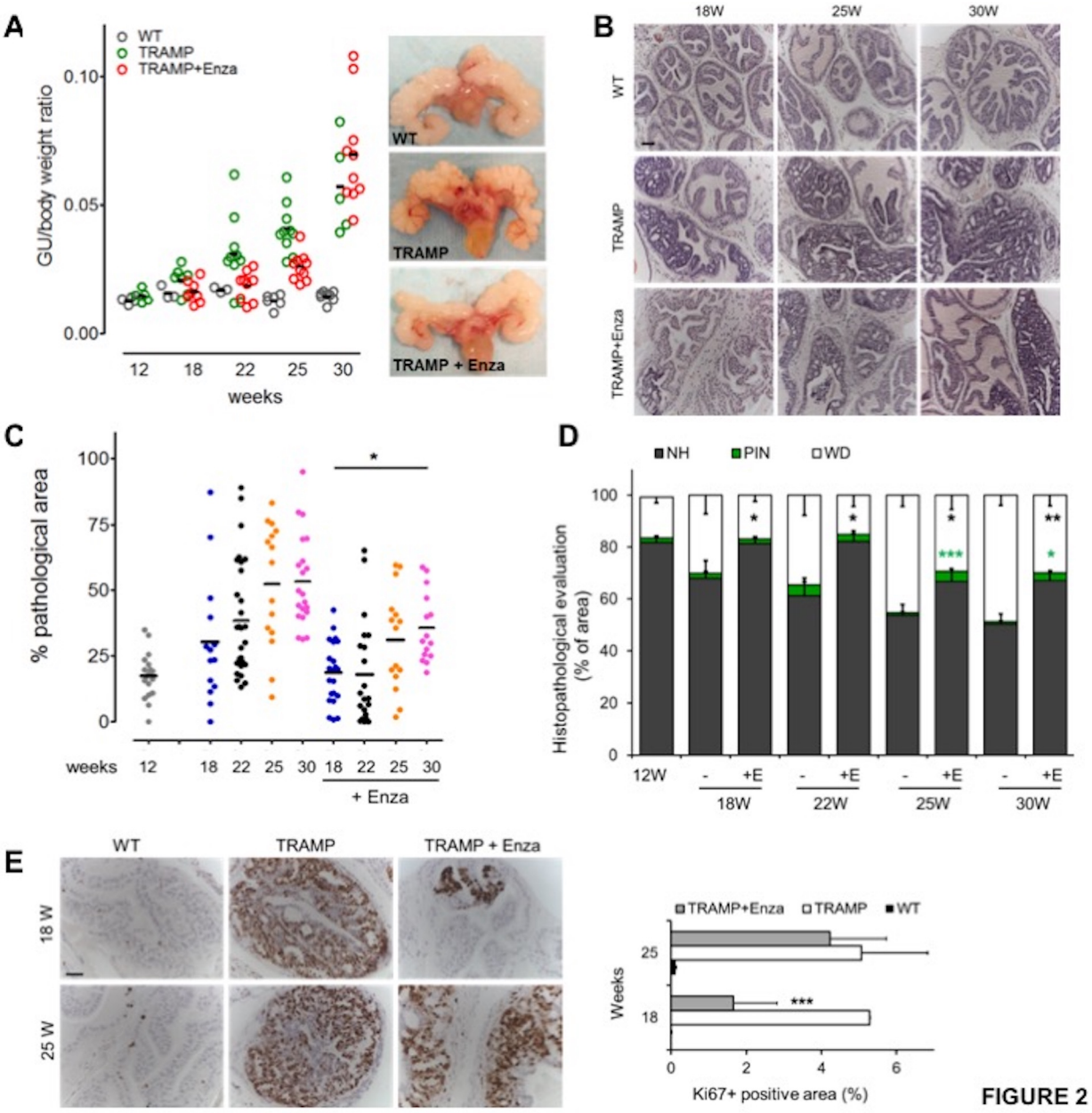
A
WT
TRAMP
TRAMP+Enza
GU/body weight ratio
0.10
0.05
0.00
12
18
22
25
30
weeks
WT
TRAMP
TRAMP + Enza
B
18W
25W
30W
WT
TRAMP
TRAMP+Enza
C
% pathological area
100
75
50
25
0
weeks
12
18
22
25
30
18
22
25
30
+ Enza
*
D
NH
PIN
WD
Histopathological evaluation (% of area)
100
80
60
40
20
0
12W
-
+E
18W
22W
25W
30W
E
WT
TRAMP
TRAMP + Enza
18 W
25 W
TRAMP+Enza
TRAMP
WT
Weeks
25
18
***
0
2
4
6
Ki67+ positive area (%)

FIGURE 2

FIGURE 3

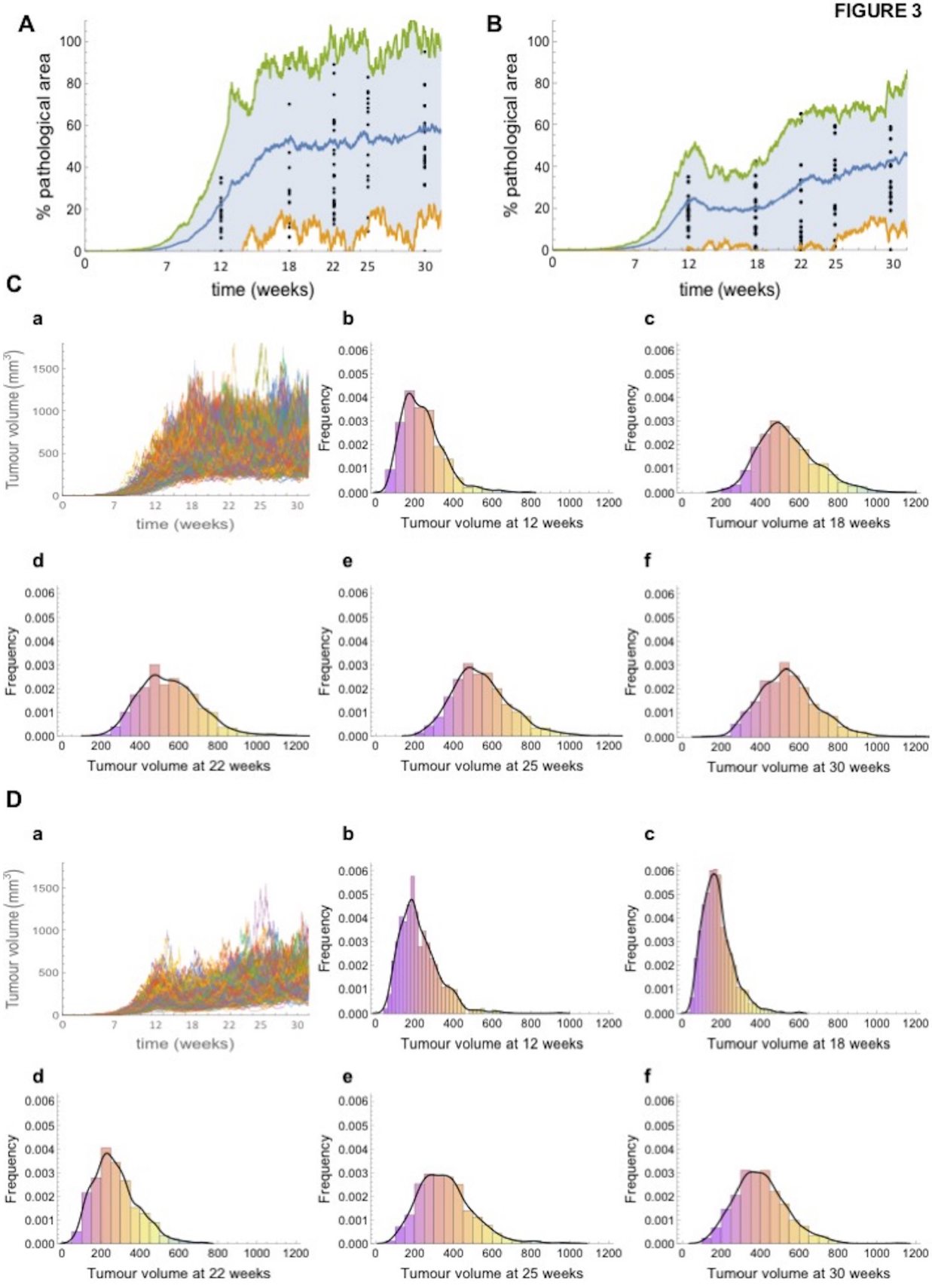
A
% pathological area
time (weeks)
B
% pathological area
time (weeks)
C
a
Tumour volume (mm3)
time (weeks)
b
Frequency
Tumour volume at 12 weeks
c
Frequency
Tumour volume at 18 weeks
d
Frequency
Tumour volume at 22 weeks
e
Frequency
Tumour volume at 25 weeks
f
Frequency
Tumour volume at 30 weeks
D
a
Tumour volume (mm3)
time (weeks)
b
Frequency
Tumour volume at 12 weeks
c
Frequency
Tumour volume at 18 weeks
d
Frequency
Tumour volume at 22 weeks
e
Frequency
Tumour volume at 25 weeks
f
Frequency
Tumour volume at 30 weeks

FIGURE 4

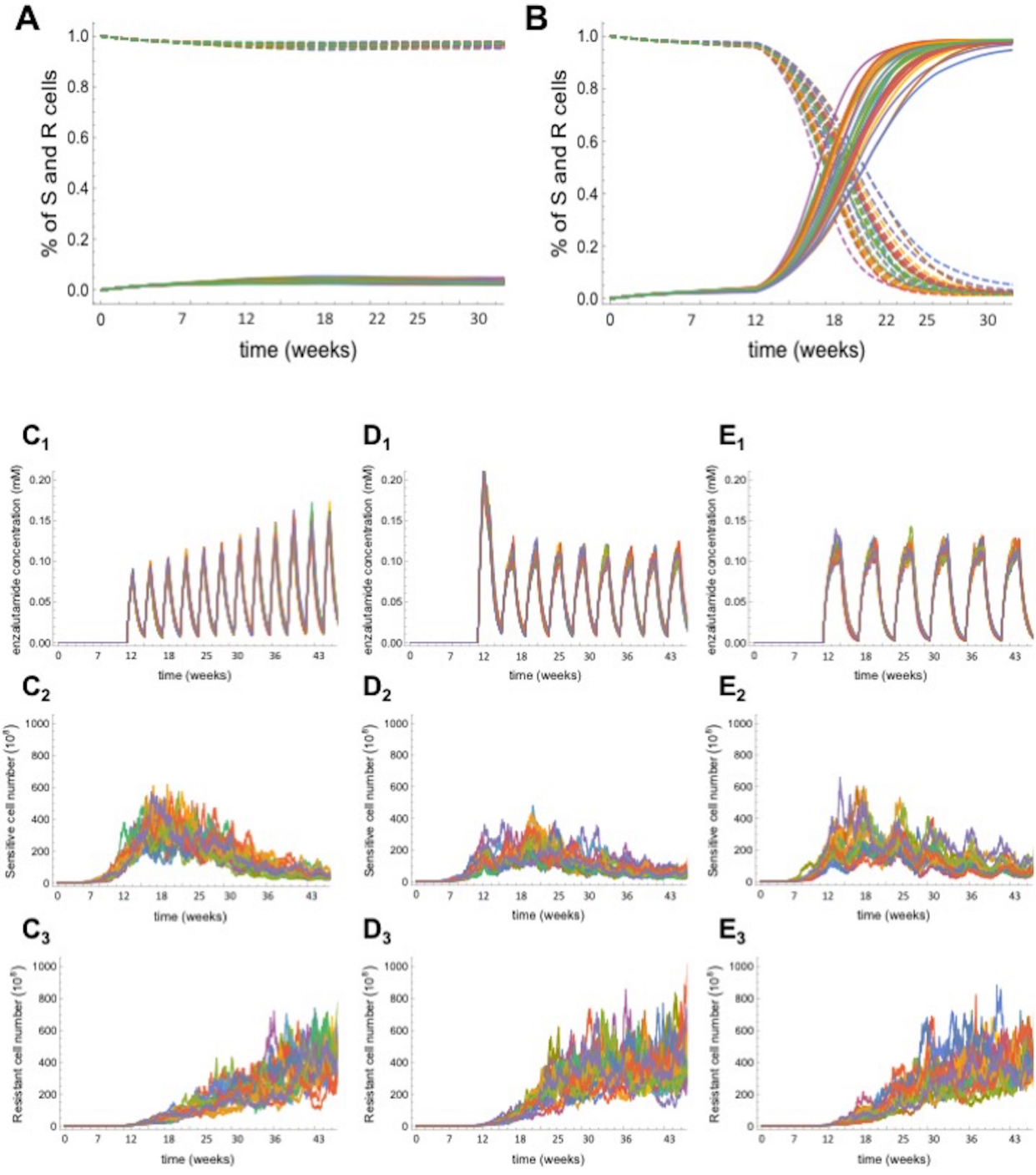
A
B
% of S and R cells
time (weeks)
C1
D1
E1
enzalutamide concentration (mM)
C2
D2
E2
Sensitive cell number (10^8)
C3
D3
E3
Resistant cell number (10^8)

FIGURE 5

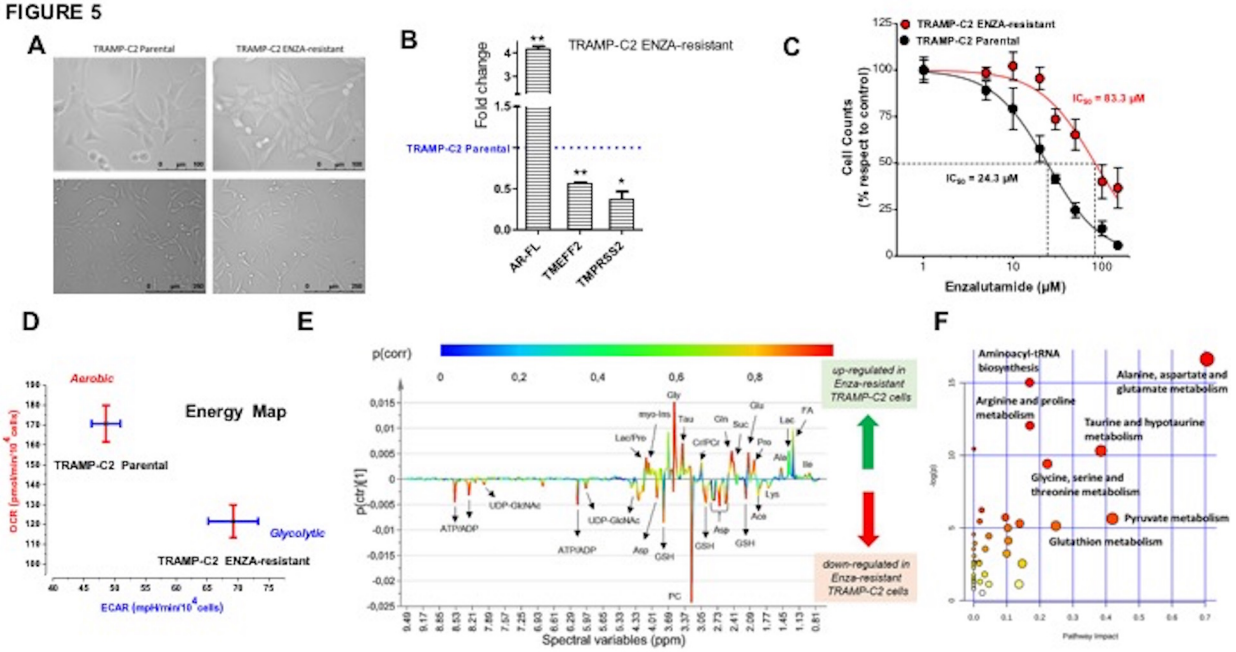
A
TRAMP-C2 Parental
TRAMP-C2 ENZA-resistant
B
TRAMP-C2 ENZA-resistant
Fold change
TRAMP-C2 Parental
AR-FL
TMEFF2
TMPRSS2
C
TRAMP-C2 ENZA-resistant
TRAMP-C2 Parental
Cell Counts
(% respect to control)
IC50 = 83.3 µM
IC50 = 24.3 µM
Enzalutamide (µM)
D
Energy Map
Aerobic
TRAMP-C2 Parental
Glycolytic
TRAMP-C2 ENZA-resistant
OCR (pmol/min/10^4 cells)
ECAR (mpH/min/10^4 cells)
E
p(corr)
p(corr)[1]
up-regulated in Enza-resistant TRAMP-C2 cells
down-regulated in Enza-resistant TRAMP-C2 cells
Spectral variables (ppm)
F
Aminoacyl-tRNA biosynthesis
Alanine, aspartate and glutamate metabolism
Arginine and proline metabolism
Taurine and hypotaurine metabolism
Glycine, serine and threonine metabolism
Pyruvate metabolism
Glutathion metabolism
-log(p)
Pathway Impact

FIGURE 6

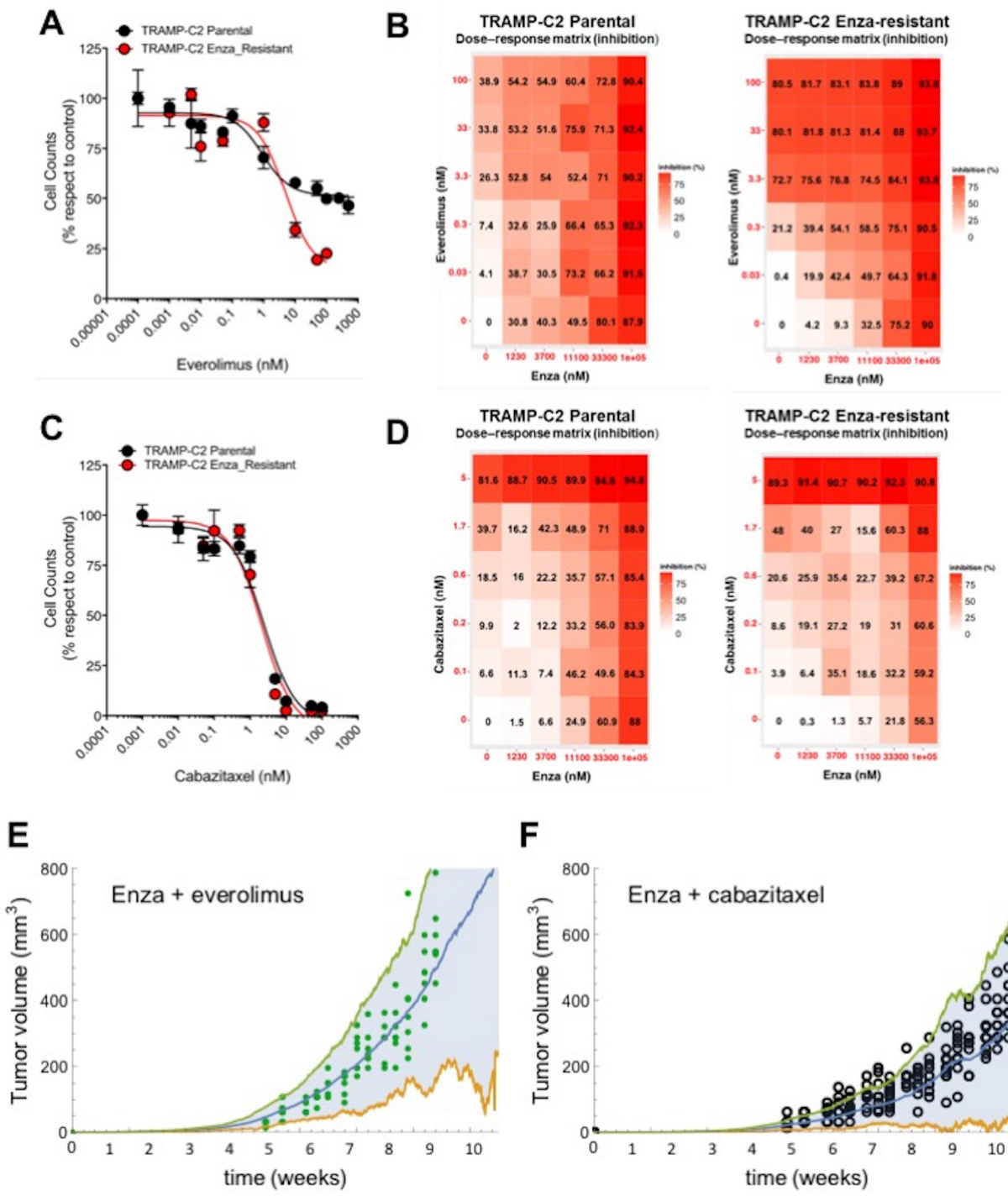
A
TRAMP-C2 Parental
TRAMP-C2 Enza_Resistant
Cell Counts (% respect to control)
Everolimus (nM)
B
TRAMP-C2 Parental
Dose–response matrix (inhibition)
TRAMP-C2 Enza-resistant
Dose–response matrix (inhibition)
Everolimus (nM)
Enza (nM)
C
TRAMP-C2 Parental
TRAMP-C2 Enza_Resistant
Cell Counts (% respect to control)
Cabazitaxel (nM)
D
TRAMP-C2 Parental
Dose–response matrix (inhibition)
TRAMP-C2 Enza-resistant
Dose–response matrix (inhibition)
Cabazitaxel (nM)
Enza (nM)
E
Enza + everolimus
Tumor volume (mm3)
time (weeks)
F
Enza + cabazitaxel
Tumor volume (mm3)
time (weeks)

FIGURE 7

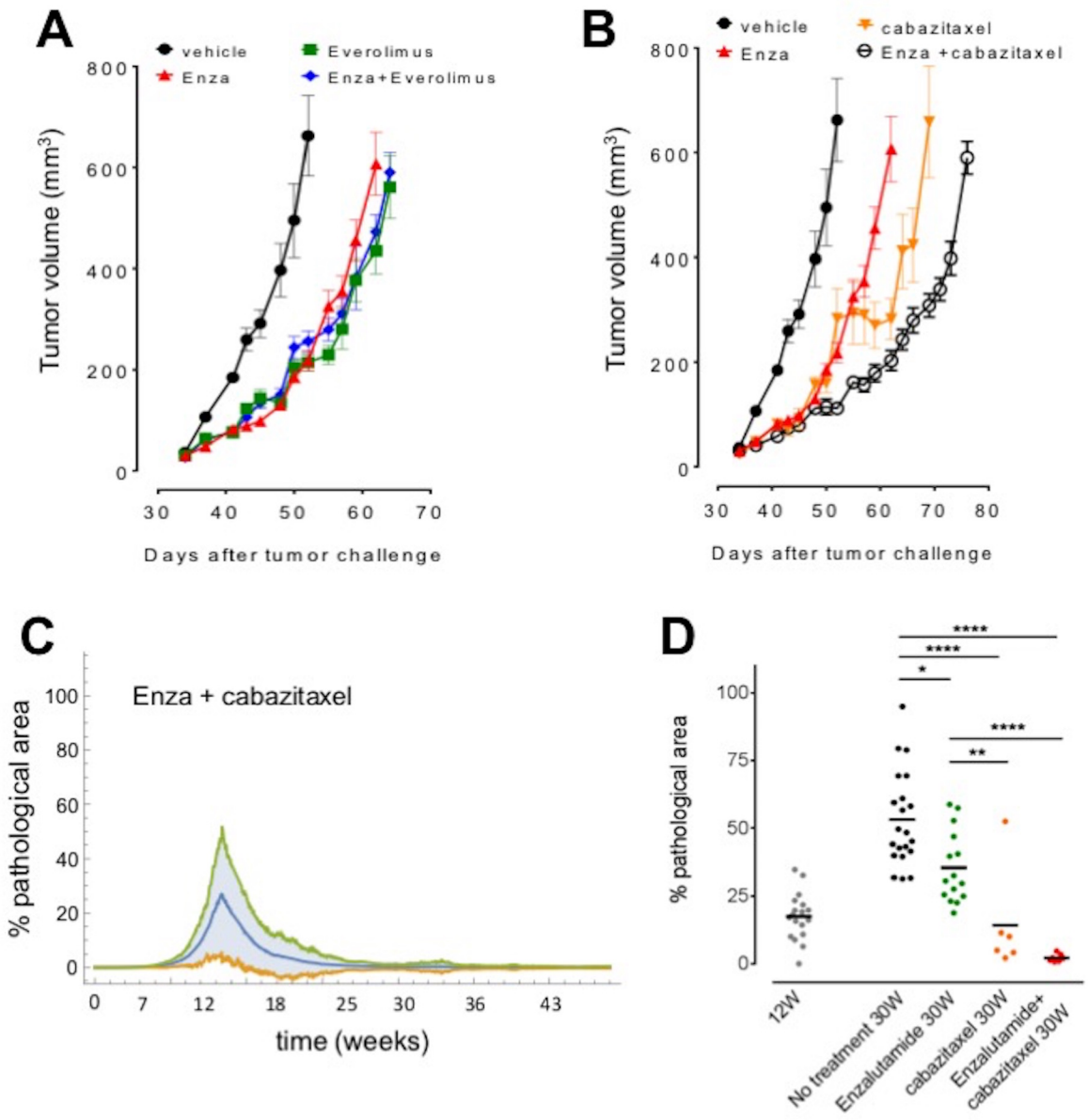
A
vehicle
Enza
Everolimus
Enza+Everolimus
Tumor volume (mm3)
Days after tumor challenge
B
vehicle
Enza
cabazitaxel
Enza +cabazitaxel
Tumor volume (mm3)
Days after tumor challenge
C
Enza + cabazitaxel
% pathological area
time (weeks)
D
% pathological area
12W
No treatment 30W
Enzalutamide 30W
cabazitaxel 30W
Enzalutamide+ cabazitaxel 30W